

Beyond power density: unexpected scaling laws in scale up of characterization of reverse-electro-dialysis membranes.

Timothée Derkenne ^a, Annie Colin^a and Corentin Tregouet^{*,a}

Abstract

Blue energy represents a large reservoir of renewable osmotic energy that can be converted into electricity by reverse electro dialysis (RED). This method is based on ion-exchange membrane. Before large scale production, these membranes are compared on very small samples on the basis of the power they enable to produce per unit area. Through a systematic study of the effect of the membrane size on the power density, we show experimentally that for classical measurement cells, the power density strongly varies with the size of the membrane: the smaller the membrane, the higher the power density. The results are explained by a theoretical modeling which describes the effect of the access resistance at the scale of the membrane. Based on this work, a few recommendations are formulated to perform scalable and meaningful measurements of membrane resistance and power density.

Key words: blue energy, nanofluidics, reverse electro dialysis, access resistance

1 Introduction

Global demand on energy is growing due to the urging necessity to switch to decarbonated energy production. Blue energy (BE), by harvesting osmotic energy from salt gradients, typically where fresh-water rivers enter the salty ocean, has the potential to be a valuable new source of energy¹. Other sources of salt gradient can arise from industrial or domestic waste water, or dedicated engineered fluids^{2,3}. It is indeed possible to generate spontaneous ionic flows through nanoporous membranes and collect this electrical energy: this process of energy harvesting is called reverse electro dialysis (RED). Considering the suitability, sustainability and reliability of the exploitation^{1,2,4-6}, the blue energy power that could realistically be harvested can be estimated as 625 TWh/year^{7,8}, which corresponds to 2.2% share of global electricity consumption in 2022⁹.

Most harvesting methods are based on ion-exchange membranes containing typically nanometric pores (1-nm pores). The main origin of cost to harvest this energy is the planar membranes. As a consequence, technologies are benchmarked in terms of power per unit area of membrane. Real-scale prototype plants reach about 1 W/m² of membrane¹⁰. The profitability threshold is estimated at 5 W/m²¹¹ (for a membrane cost around 2\$/m²). At present, the price of the cheapest selective membranes in SPEEK is still higher than 10 euros per m²¹². The technology is therefore still a long way from economic viability, and needs to be improved.

Over the last ten years or so, numerous studies have focused on the synthesis of new membranes and their improvement to overcome this barrier¹³⁻¹⁵. Most of the innovative membranes

are characterized in the labs by the power per unit area (power density) on devices with a membrane area of the order of 10 μm², assuming that for given fluids, the power density depends only on the membrane material and thickness, and will be poorly affected by the scale-up. This is justified by the assumption that the measured resistance in the experimental device corresponds to the one of the most resistive object, i.e. the membrane. The power density of the membrane is thus calculated by dividing the harvested power by its area.

Recent literature reviews show a correlation between membrane area and power density and call this hypothesis into question¹⁶⁻²⁰. Some of the phenomena behind these measurements are easy to understand. The ionic resistance of the experimental device is due not only to the membrane, but also to its surroundings, in particular the electrolyte reservoirs. As an example, when the membrane size is increased, the membrane resistance get smaller and can even become smaller than the resistance of the reservoirs (independent of the membrane area). In such a situation, as the size of the membrane would increase, in the situation where the surroundings are unchanged, the power recovered would remain constant and the density power (power by membrane area unit) would decrease. Other possible effects are more complex. The spatial distribution of ions in the electrolyte can be affected by the selectivity of the membrane, the geometry of the device i.e. membrane size, electrode size, distance between electrodes and membranes.

In this paper, the relation between membrane area and power density is systematically investigated for a given commercial membrane (Nafion 115) in a standard electro-chemical cell. In a first part (section 2.1), the cell resistance is measured with respect to the membrane area with the same salt concentration on both sides of the membrane. In a second part (section 2.2), resistance and produced power are measured with different salt concentrations

^a ESPCI Paris, PSL Research University, MIE-CBI, CNRS UMR 8231, 10, Rue Vauquelin, F-75231 Paris Cedex 05, France.

* Corresponding author: corentin.tregouet@espci.psl.eu

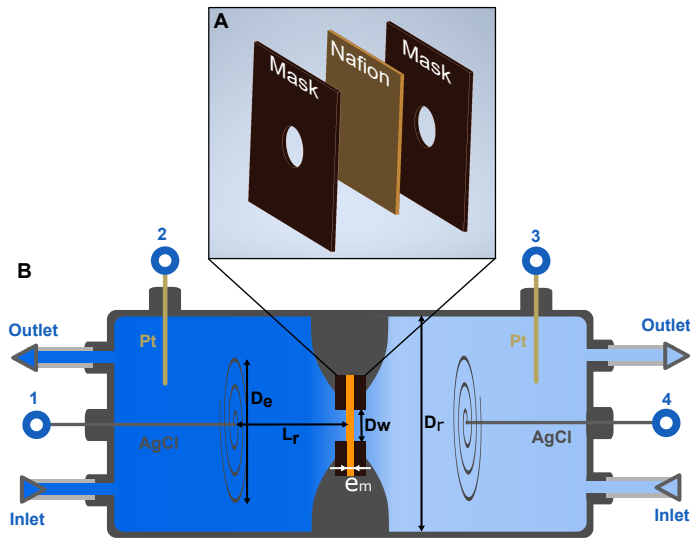


Fig. 1 Experimental set up used for all the measurements. (a) 3D view of the membrane (yellow square) mounted between two mylar masking windows (red square with a circular hole). The size of this hole defines the effective $S_{membrane}$ taken into account. (b) Schematic of the cell with the two reservoirs of salt solutions, with inlet and outlet. The two silver chloride electrodes made of a wire spiral (labels 1 and 4). The membrane (orange) fixed in a mounting bracket with a masking window on each side (black). Two platinum wires (labels 2 and 3) are placed behind the silver chloride electrodes. Electric circuit are presented SI. Geometrical parameters are indicated in Table 1.

on both sides of the membrane. These results are then discussed (section 3) in comparison with the literature, and implications are drawn for further research.

We mainly highlight two phenomena: 1- the conductance is not proportional to the membrane surface, but to its square root for classical electro-chemical cell dimensions; 2- as a consequence, the maximum power density strongly decreases with membrane size. As a result, extrapolation of power density from measurements on small membranes is flawed and overly optimistic.

2 Results

An electro-chemical cell (Figure 1) was designed to measure Nafion-membrane characteristics (Nafion 115). The Nafion membrane is clamped between two masking windows to vary the membrane effective surface from 10^{-2} to 10^2 mm^2 . This assembly (membrane and masking windows) divides the electro-chemical cell into two reservoirs. As shown in Figure 1, from each side come the water inlet and outlet, the silver-chloride electrodes and the platinum electrodes (more details in the Methods section)

Cell electrical resistance R_{cell} , open-circuit voltage E_{OCV} and maximum power P_{max} were measured for varying membrane surface and salt solutions. Salt solutions (labeled 1, 2 and 3) consist of potassium chloride of varying concentrations: solution 1 has a concentration $c_1 = 1 \text{ g/L}$ ($1.7 \cdot 10^{-2} \text{ M}$) and a conductivity $\sigma_1 = 1850 \mu\text{S/cm}$; solution 2 has a concentration close to $c_2 = 10 \text{ g/L}$ ($1.7 \cdot 10^{-1} \text{ M}$) such as $\sigma_2 = 10 \cdot \sigma_1$; solution 3 has a concentration close to $c_3 = 100 \text{ g/L}$ (1.7 M) such as $\sigma_3 = 100 \cdot \sigma_1$ (more details in Methods section).

Electrical measurements are performed using a 2-electrode con-

figuration and a 4-electrode configuration. With two electrodes only, the potential is measured at electrodes in which current is flowing. In some conditions (discussed in the Method section), these electrodes are therefore submitted to polarization at the interface, inducing an excess resistance²¹ which depends on salt concentration. Consequently, at high concentration (c_2 and c_3), when the bulk resistance is low, the electrode polarization resistance is of the same order of magnitude as the total resistance. To overcome this issue, the 4-electrode configuration enables a voltage measurement on electrodes through which there is no current, and hence no effect of the polarization resistance. In the conditions where there is no effect of electrode polarisation, the 2-electrode configuration is used. More details on the setup and the measurement protocol are given in the method section.

2.1 Resistance

2.1.1 Experimental results

In this first section, resistance measurements are performed for symmetrical configurations (same salt concentration in the two reservoirs, and hence no gradient).

In a first step, the cell resistance is measured with solution 1 ($c_1 = 1 \text{ g/L}$ ($1.7 \cdot 10^{-2} \text{ M}$)) for various membrane areas. As shown in Figure 2, these measurements yield a decreasing resistance with respect to the membrane area, which can be approximated by a power law $S_{membrane}^{-1/2}$. This scaling is a very good agreement with the measurements of Lin et al.²⁰.

The same scaling law is obtained with solution 2 ($c_2 = 10 \text{ g/L}$ ($1.7 \cdot 10^{-1} \text{ M}$)), with a resistance 10 times lower. For larger concentration ($c_3 = 100 \text{ g/L}$ (1.7 M)), a lower resistance is observed, with a deviation from the power law $S_{membrane}^{-1/2}$. Furthermore, as shown on Figure 2A for solution 1, increasing the length of the reservoirs by a factor 4 barely affects the resistance, showing that the measurement is not sensitive to the reservoir.

In a second step, the cell resistance is measured without membrane, but with the masking windows (in this case, we keep the notation $S_{membrane}$ to describe the opening area in the masking windows). Results are shown in Figure 2B for solutions 1, 2 and 3. The three set of measurements show a decrease of the resistance with the opening area with a power law $S_{membrane}^{-1/2}$ over 4 decades of area. More precisely, for the solutions 1 and 2, the measured resistance is the same with and without membrane. The measurements with solution 3 show the same scaling law as for solution 1 and 2, on the contrary to the measurements with a membrane.

2.1.2 Theoretical modeling

These results seems in contraction with the textbook usual equation of resistance R which states:

$$R_{membrane} = \frac{1}{\sigma_m} \cdot \frac{e_m}{S_{membrane}} \quad (1)$$

(with e_m the membrane thickness, σ_m the conductivity of the membrane, and $S_{membrane}$ its surface) which would yield a power law $R_{membrane} \propto S_{membrane}^{-1}$.

Green et al.^{22,23} have shown that for a perfectly selective nanopore and for a non-selective nanopore connected to two reser-

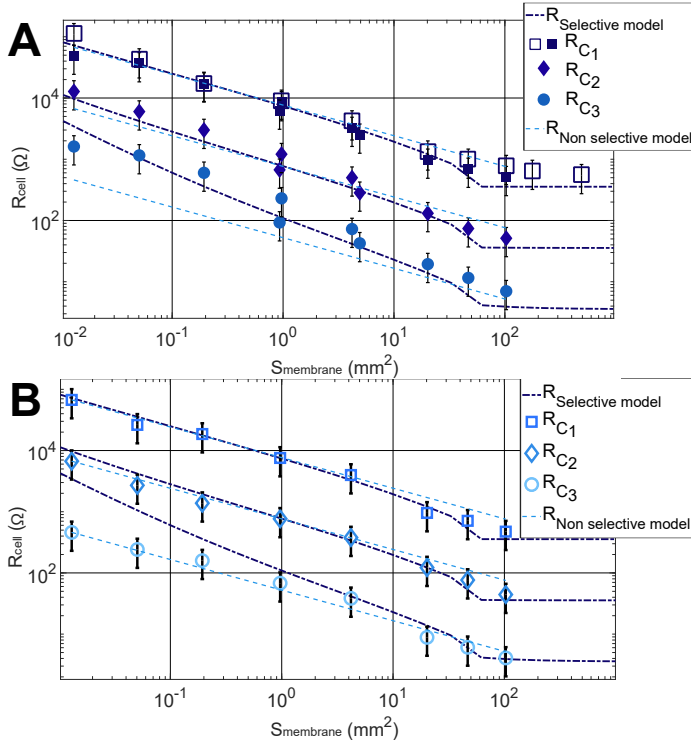


Fig. 2 Measured electrical resistances (R_{cell}) with respect to the membrane area ($S_{membrane}$) for varying geometries in symmetrical configurations. (a) With a Nafion membrane (solid symbols): the measured resistance follows the model developed by Green *et al.*^{22,23} (black dashed lines). Open symbols are for a different geometry (L_2 instead of L_1), as expected no influence of the reservoir length is observed. (b) Without membrane (open symbols): resistance follows the model which shows a trend in $1/\sqrt{S_{membrane}}$ (light blue dashed line). Dashed lines from the model are the same in A, B and the same as in Figure 3.

voirs, the total resistance can be split in 5 as presented in Figure 3: the resistances of the two reservoirs on both sides, the resistance of the nanopore, and the access resistances at the two reservoir/nanopore connections:

$$R_{cell} = R_{res,left} + R_{access,left} + R_{nanopore} + R_{access,right} + R_{res,right} \quad (2)$$

The reservoir resistance is $R_{res,k} = \frac{1}{\sigma_i} \cdot \frac{L_{res,k}}{S_{res,k}}$ ($k = left, right$), with σ_i the electrolyte conductivity ($i \in 1, 2, 3$), $L_{res,k}$ the lengths of the reservoirs, and $S_{res,k}$ their cross-section areas. The nanopore resistance writes $R_{nanopore} = \frac{1}{\sigma_{nanopore}} \cdot \frac{L_{nano}}{S_{nano}}$, with $\sigma_{nanopore}$ the conductivity of the nanopore (which takes into account both the cations and counter-ions), L_{nano} its length, and S_{nano} its cross-section area. While the nanopore from the initial model and the present membrane are different in geometry, they share the same permselective trait and therefore we treat them as they same and denote both as "membrane", and use Eq (1).

The access resistances originate from the mismatch between the two section areas $S_{res,k}$ and $S_{membrane}$ (S_{nano} in the original paper), which imposes a convergence/divergence of field lines. There is no simple equation in the general case, but it has been modeled for arbitrary geometries by Green and collaborators^{22,24},

and a simple equation has been proposed for an infinite reservoir ($S_{res,k}/S_{membrane} \rightarrow \infty$) and a circular nanopore by Hall²⁵:

$$R_{access,asymptotic} = \frac{1}{\sigma_i} \cdot \frac{\sqrt{\pi}}{4\sqrt{S_{membrane}}} \quad (3)$$

As explained by Green *et al.*^{22,23}, the origin of the access resistances is purely geometrical, and it exists anytime $S_{membrane} \neq S_{reservoir}$.

The model of Green can thus be applied to the current system by replacing the nanopore by the membrane. The selectivity of the membrane is assumed to be high enough to allow for the decomposition of the total resistance in five as explained above. The access resistance therefore depends on the membrane area and shows an asymptotic scaling $R_{access} \sim \frac{1}{\sigma\sqrt{S_{membrane}}}$ for $S_{membrane}/S_{res} \ll 1$. The nanopore resistance becomes the membrane resistance described by Eq (1). Finally, the reservoir section considered to model our system is the section of the electrodes.

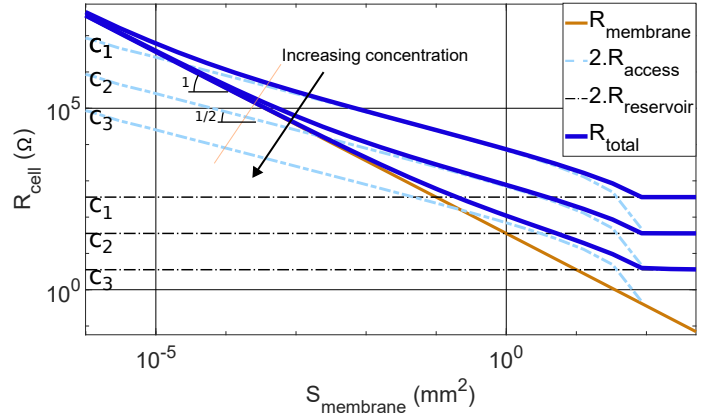


Fig. 3 Evolution of the resistance with respect to the membrane size according to the developed model (with a perfectly selective membrane). The system is theoretically described by 5 resistances in series with differential scaling with size. Curves are calculated for a symmetrical salt concentration c_1 , c_2 and c_3 . The membrane resistance ($R_{membrane}$) is considered independent of the salt concentration, based on Avci *et al.*²⁶.

Hence, once the Nafion membrane is assumed to be perfectly selective, the 5 resistances of Eq (2) are known with the Nafion resistivity as only adjustable parameter, and sum up to yield the total resistance. Nafion-resistivity measurement from literature show poor variations with concentration²⁶. The resistance is therefore chosen independent of concentration for simplicity. The best agreement between the model and experiments is found for a Nafion resistivity $R_{membrane} \cdot S_{membrane} = 0.35 \Omega \cdot \text{cm}^2$. It is reasonable agreement with the values found in literature, considering the variability between the different reported values²⁶⁻²⁸.

As shown in Figure 3, the total resistance versus membrane area shows a power law $S_{membrane}^{-1/2}$ which indicates that the total resistance is dominated by the access resistances in the range of membrane surface considered here. This explains why the total resistance does not depend on the presence of the membrane, except at high concentration and small membrane area when the membrane resistance begins to be of the same order as the access resistance. This also explains why the total resistance does not depend on the

reservoir length.

This model describes very well the experimental results for the different areas and solutions, as visible in Figure 2. This indicates that in this simple usual configuration, the resistance is dominated by the access resistance. As a consequence, the total conductance ($1/R_{total}$) does not scale linearly with the membrane surface.

The modeling on a broader range of membrane areas (Figure 3) shows that at very small membrane areas, the resistance should be dominated by the membrane resistance, and that on the opposite, when the membrane area becomes as large as the reservoir area, the total resistance should be dominated by the reservoir area.

2.2 Power

Now that the effect of membrane size is understood for homogeneous cells, asymmetric configurations can be investigated. To this aim, different concentrations are introduced in the left and right reservoir. One always contains solution 1, and the other contains solution 2 or solution 3. This introduces a concentration ratio of 10 or 100 between the two sides of the membrane. Due to the selectivity of the membrane, this creates a potential difference, and a current if the electrical circuit is closed by a resistor.

The power that is injected in an external load resistance R_{load} depends on the internal resistance R_{cell} and the open-circuit voltage E_{OCV} through the voltage divider:

$$P(R_{load}) = E_{OCV}^2 \cdot \frac{R_{load}}{(R_{load} + R_{cell})^2} \quad (4)$$

The maximum power is then reached when $R_{load} = R_{cell}$:

$$P_{max} = P(R_{load} = R_{cell}) = \frac{E_{OCV}^2}{4R_{cell}} \quad (5)$$

The maximum power measurement can therefore be found by measuring the power for various R_{load} (small symbols in Figure 4C), or by measuring R_{cell} (Figure 4A) and E_{OCV} (Figure 4B), yielding the power shown by the dashed lines and large triangles in Figure 4C).

Measurement of the open-circuit voltage (OCV) E_{OCV} (Figure 4B) shows a significant variation with the membrane area: decreasing the membrane size induces a decrease of the OCV. This result is very surprising since for given solutions, the OCV is expected to be a function of the membrane selectivity only, and hence independent of the resistance and membrane size. Although the author has no clear understanding of this effect so far, these results may be related to the effect observed by Yazda *et al.*²⁹ for solid-state selective nanopores: they observed that when nine 4-nm wide nanopores come closer to each other, the OCV drops below a 500 nm distance.

This effect could be due to the concentration field close to the membrane which arises from the very low (but non zero) osmotic flux of ions through the membrane (due to the non-ideal selectivity of the membrane), and which is called concentration polarization. This hypothesis is coherent with the observation that thicker masking windows lead to a stronger decrease of the OCV, as shown in SI.

Measurements of the cell resistance are displayed on Figure 4A. Cell resistance measurements are shown in Figure 4A. The values

measured when the two tanks contain two different salinities (solution 1 and 2 or solution 1 and 3) are close to half the sum of the resistances of the two tanks containing the same solution. This means that cell resistance varies as $S_{membrane}^{-1/2}$ at least for membranes with surfaces greater than 10^{-1} mm^2 . This means that the ion-concentration profile is not very different in the two cases, or at least that the concentration profile in the dilute zone is not greatly affected by contact with a more concentrated tank. Remember that the cell resistance is largely controlled by the resistance of the compartment containing the more dilute solution. We note that this agreement is less good when the membrane surface is smaller. This situation corresponds to the case where the open circuit potential drops and reaches values less than 70 mV in the situation of solution 1 and 2 or 150 mV in the situation of solution 1 and 3. In those situations, it is reasonable to assume that the previous remark on the concentration profile in the diluted zone is not valid, and that it is affected by the fact that the diluted reservoir is in contact with a concentrated reservoir. Note that the resistance is 4 times smaller than the half-sum of the resistances, which implies a significant change in the concentration profile. This indicates even more that the measurement of the membrane selectivity could also be affected by size effects and the cell geometry, which would also hinder the comparison of data from literature. It is hence difficult to deduce the selectivity of the Nafion membrane from these experiments.

The power density (power per unit area of membrane $P_{max}/S_{membrane}$) is then plotted as a function of the membrane area $S_{membrane}$ in Figure 4D and it appears that the power density does depend on membrane area. The relation between power density and membrane area yields a power law with an exponent $-1/2$. From Equation (5), it is clear that the result from section 2.1 ($R_{cell} \propto S_{membrane}^{-1/2}$, which is still valid in the asymmetric configuration when surface membranes are greater than 10^{-1} mm^2 as visible in Figure 4A), yields a scaling law for the maximum power: $P_{max} \propto S_{membrane}^{1/2}$. From this, it is straightforward that the power density has a scaling law $P_{max}/S_{membrane} \propto S_{membrane}^{-1/2}$. For membrane size values smaller than 10^{-1} mm^2 , it seems that the scaling in $S_{membrane}^{-1/2}$ is still valid. This is due to a compensation phenomenon that we can't yet explain by the models. In this zone, the resistance is lower, but the circuit potential is not constant, but falls relative to the reference value.

As visible in Figure 4D, two sets of measurements performed on reservoirs of different lengths (L_1 and L_2) yield exactly the same results. This proves that the deviation from the usual assumption of constant power density is indeed due to the access resistance which dominates the total resistance of the device. This modeling also explains the trend observed by previous work from literature^{19,20}.

These results show that the size of the membrane does have an impact on the maximum power density that can be extracted: without precise analysis of the equivalent electrical circuit or a universal measurement protocol, the maximum power density should not be considered as an intrinsic parameter of the membrane, and is therefore not scalable from small scale experiments to larger scale.

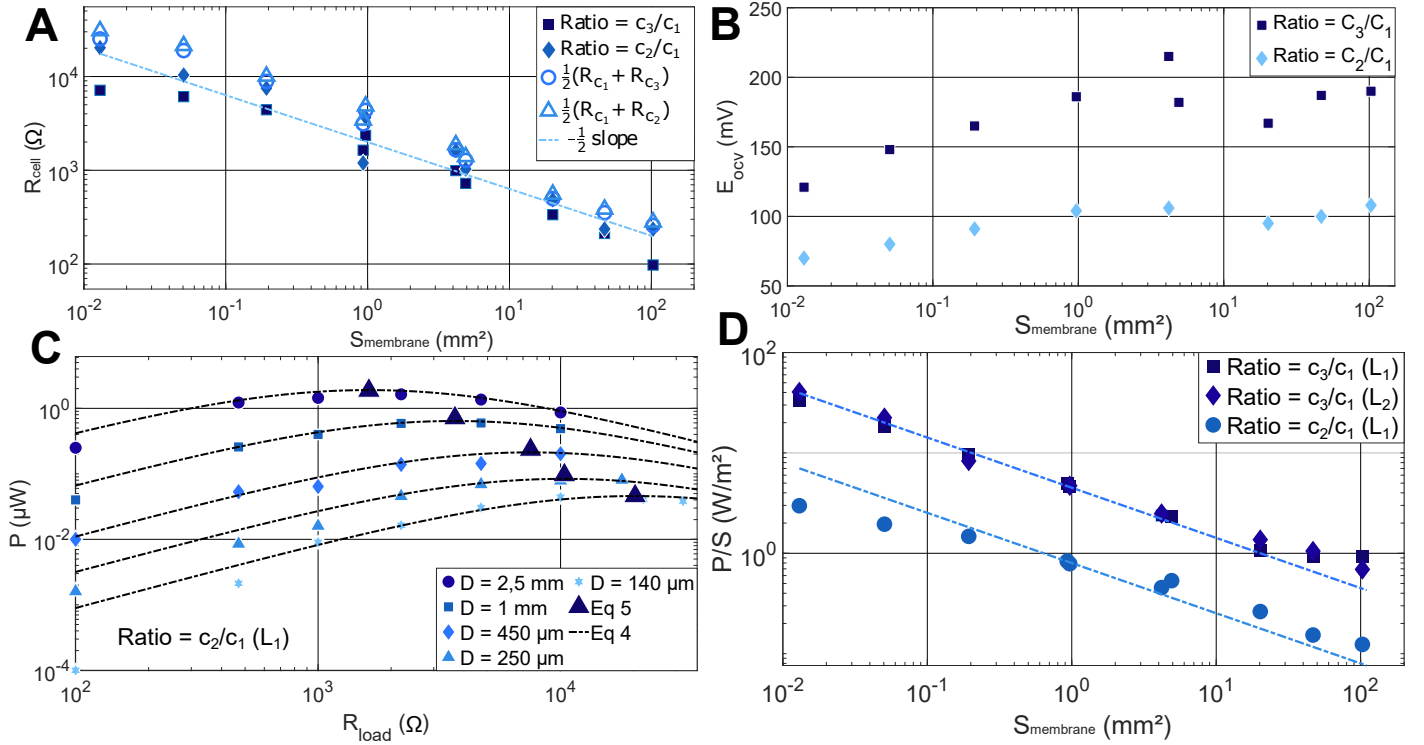


Fig. 4 Measured power when the membrane is placed between reservoirs of different salinity. (a) Measured cell resistance (R_{cell}) for a varying $S_{membrane}$ for salt ratio of 10 and 100 (solid shapes). Open shapes are calculated from Fig 2 assuming that the ratio configuration is half of c_1 resistance and half of c_3 resistance. Light blue dashed line is a $-1/2$ slope guide for the eyes. (b) Variation of the open-circuit voltage (E_{ocv}) with the membrane area ($S_{membrane}$): the OCV does not vary for large membranes, but drops at small areas. (c) Generated output power (P) as a function of the load resistance (R_{load}) for a salt ratio of 10: the maximum defines the maximum power density, in good agreement with the values calculated from Eq (5) (solid triangles). Dashed line is the curve predicted by the cell resistance and OCV measurement from Eq (4). (d) Maximum power density ($P_{max}/S_{membrane}$) vs $S_{membrane}$ shows a power-law decrease with exponent $-1/2$. Measurements have been done for two electrode-membrane distances L_1 and L_2 , with the same result.

3 Discussion

These results raise several difficulties for membrane characterisation, literature analysis, and scale up.

First, this implies that membrane characterization must be done in carefully-chosen geometry to ensure that the dominating resistance (among the reservoir, access, and membrane resistances) is the one of interest. To probe the membrane, the access resistance and the reservoir resistance must be lower lower than the membrane resistance. This can be achieved by using electrode of the same size as the membrane, and as close as possible, possibly in contact with the membrane.

Second, in this work, we have demonstrated that each of the three terms contributes to the overall response of the system. While conducting a literature survey, to our dismay, we discovered that it is often the case that experimental papers do not provide enough details on the geometric setup. Namely, what is the size of the membrane (usually indicated), but also the size of the electrodes and the distance between the electrodes and the membrane (usually not indicated). Thus, we emphasize to future experimentalists the importance of providing a detailed description, even in the supplementary material, of the setup, and all geometrical parameters.

Finally, we emphasize that our work has focused on a simpli-

fied system which has only one membrane, used to characterize membranes. In applied systems, there is a stack of membranes separated by spacer of typically 100 μm . We provide two strategies on how we believe the resistance and power densities measured on single membranes can be scaled up to predict their performance in applied systems (stacks). A first option is to keep membrane and electrodes separated by $L_{spacer} = 100$ μm , and have roughly the same diameters for electrodes and membrane ($D_{electrode} \simeq D_{membrane}$), and have them significantly larger than 100 μm . A second option is to have smaller membrane, as far as $D_{electrode} = D_{membrane}$ and $L_{spacer} \ll D_{membrane}$. Doing so, the power density measured should be meaningful and scalable.

Due to this artefact, power densities measured in other configuration can yield very high values of power density³⁰⁻³³, which are not relevant in the scope of large-scale energy harvesting.

4 Conclusion

To conclude, this systematic study on the effect of the membrane size for reverse electro-dialysis shows that when the electrodes are larger than the membrane, the resistance does not scale inversely with the membrane area, but with its square root. This is well understood by taking into account access effects at the entrance of the membrane. It results that the power density depends on the membrane size. As a consequence, without being very careful on

the electro-chemical cell design, measurements of power densities on small membranes are overly optimistic and cannot be scaled up to predict the power density in a membrane stack.

5 Methods

5.1 Salt solutions

Salt solutions were prepared using high-purity potassium chloride (Sigma-Aldrich) and Milli-Q deionized water. K^+ and Cl^- have almost the same diffusivity.

The conductivity were measured using a conductimeter (MU 6100H VWR) at room temperature for all the solution to prevent the activity to be modified by the endothermic mixing reaction.

5.2 Membrane preparation

Nafion 115 membrane needs to be prepared to ensure its maximum performances and stability. Needed pieces were cut from the Nafion sheet (Fuel Cell Store) and placed in deionized water for at least 24 hours before use. This ensures that all the hydrophilic negatively charges SO_3^- sites of the polymer are filled with water. The hydrated salt is therefore able to cross it³⁴.

Results are not affected when the soaking solution is of the same concentration than the solution used during the experimentation (in symmetrical condition without concentration gradient). For concentration-gradient measurement, the membrane is prepared in salt solution of the low concentration (1 g/L).

5.3 Electro-chemical cell

An electro-chemical cell (Figure 1) was designed and 3D printed (clear resin V4, Formlabs 3B⁺). The Nafion membrane with the two masking windows was clamped in a mounting bracket. It was then pressed between two O-ring in the middle of the cell by the two screwable reservoirs. From each side come the water inlet and outlet, the silver chloride electrode and the platinum electrode. Tubings and wires are connected to the cell using screwed mounting tip (Nanoport). Teflon tape is added when needed for the water sealing. Relevant sizes of the cell are listed in Table 1.

Silver electrodes are used as working electrodes and counter electrodes. When needed to solve electrode-polarization issues, platinum electrodes are used to measure the potential of the solution, while the current flows through the silver-chloride electrodes.

Silver chloride electrodes are made with a spiral-shaped 1mm-diameter silver wire (Figure 1 B). For each electrode, the outer diameter of the spiral is 1,5 cm and the total surface area is 1 cm². The silver wire was polished with sandpaper and cleaned with ethanol and deionized water. It was then placed in a beaker with highly concentrated NaCl solution. A carbon counter electrode allows to perform a chronopotentiometry measurement: a current of 15 mA is imposed while measuring the potential difference until it reaches 1,8 V. At this point, the electrode is completely covered with silver chloride. With a razor blade, part of this deposit is scratch to recover the silver. This ensures that both silver and silver chloride are in contact with the solution to allow the electrode to work as a faradaic electrode.

5.4 Masking windows

Masking windows were laser cut in a 125 μm thick Mylar sheet (Figure 1 A). Two sets of windows were prepared. One with holes between 140 μm and 2,5mm (Mylar external size is 3x3 mm) and the other between 1mm and 10mm (Mylar external size is 11x11 mm). 1mm and 2,5mm sizes are in both sets to ensure a reliable continuity of the data sets.

The free area of the window defines the effective area of the membrane. The table in annex gives the average area of the two windows of the same intended size. All the windows are circular except for the 10x10 mm which is a square.

A quick study has been made to compare the results with a window only on one side of the membrane or on both sides. Because of the isotropic properties of Nafion³⁵, the ion conduction isn't in straight line inside of

Name	Description	Size
D_r	Inner reservoir diameter	29 mm
L_r	Length between the electrode and the membrane	$L_1 = 3\text{mm}$ (default value, unless otherwise specified) $L_2 = 13\text{mm}$
V_r	Volume of the reservoir	10 mL
D_e	Diameter of the electrode	$D_1 = 1\text{cm}$ (default value, unless otherwise specified) $D_2 = 2\text{cm}$
S_e	Surface of the electrode	1 cm ²
D_w	Diameter of the masking window	[140 μm ; 10 mm]
$S_{membrane}$	Surface of the masking window, equal to the surface of the useful membrane	[0,013 ; 103] mm ²
e_m	Membrane thickness	100 μm

Table 1 Relevant sizes and geometrical parameters of the electro-chemical cell.

the membrane. Therefore, when only one window is used, the flux in the membrane will take place in a volume which have a cross section larger than the hole in the masking window. To be closer to the ideal case of a membrane of the exact size, two windows are placed on each side of the Nafion sheet. The conduction is still not completely straight. But the deviation might be lower than the membrane thickness and hence smaller than the windows diameters.

Due to the laser cutting precision and the handling variations, some misalignment between the windows could happen. It was statistically measured to be under 100 μm . Thanks to the isotropic properties of pristine Nafion³⁵, this positioning error could not induce an increase of membrane effective thickness larger than 41% in the worst case. This would increase the membrane resistance value by the same ratio. We assume that it has a very minor effect in our study.

5.5 Electrical circuit

Electrical measurements were performed using a potentiometer (BioLogic SP 300). This device has 5 wires per channel: Sensing electrode 1 (S1), Sensing electrode 2 (S3), reference electrode (S2), Working electrode (P1) and counter electrode (P2). The reference electrode S2 is always connected to the sensing electrode S1.

When silver-chloride electrodes are crossed by a current, a complex concentration polarization and capacitive double layer can take place around them²¹, which increase the measured resistance. This effect can be avoided by using 4 electrodes (Platinum electrodes in addition to the silver-chloride electrodes), or by using configurations when the electrode polarization is either absent or negligible. In the first configuration (4-electrode setup), the two platinum wires are used as sensing electrodes (connected to S1, and S3) (see SI for more detailed information). No current is going through them, they only measure the potential drop between the two reservoirs. The two silver-chloride electrodes (connected to P1 and P2) are used to inject current through the device. Therefore, the sensing and the current conduction are separated and there isn't any polarization issue on the sensing electrodes. This measurement setup is used to measure the cell resistance with or without salt ratio.

The second configuration (2-electrode configuration) is used to measure the open circuit voltage (E_{OCV}) of the cell with a concentration gradient and its response to an external load resistor (R_{load}). In those cases the voltage measurements are performed on the working- and counter electrodes. During E_{OCV} measurement, no current is going through the circuit, and

hence no capacitive double layer is created on the electrode surface. During the measurements with varying R_{load} , the high resistance of the dilute reservoir (which is highly resistive and is too dilute to create a significant capacitive double layer) dominates the overall resistance: consequently in this specific case, the variation of the high-concentration reservoir due to the polarization do not affect the total resistance. Therefore, in both cases the previously-mentioned issue with silver chloride electrodes has no effect on the measurement.

5.6 Measurement protocol

For all the presented measurements, salt solutions, membrane, electrochemical cell, masking windows and electrical circuit are prepared as explained before. The resistance measurement is made in the 4-electrode configuration (see Supp Mat for more details). Each side of the cell is filled with water using a peristaltic pump (LongerPump BT 100-1L), either with the same salt concentration on both sides (symmetric condition), or with a different concentration (gradient condition). In this last configuration, the ratio value is defined as the activity ratio (equal to conductivity ratio) between both reservoirs (Ratio = 10 or 100). When there is no air in the cell any more, the pump is stopped. To ensure that there isn't any pressure differences and parasite flows inside of the cell, measurements start only after a relaxation time of a few minutes. Once a steady state in potential is reached, the measurement begins.

To measure the resistance, the potentiostat applies a constant current I_{mes} during 10s to the cell through the silver chloride electrodes (P1 and P2). The response is a potential increase (E_{mes}) measured by the platinum wires (S1 and S3). This operation is done with 3 different I_{mes} values (100 μ A, 50 μ A and 10 μ A) with a relaxation time of 30 s between each measurements. The linear regression of the curve $E_{mes}-I_{mes}$ gives the cell resistance R_{cell} . R_{cell} is measured with this protocol for all windows sizes, with or without concentration gradient.

For the study with a concentration gradient, the value of E_{OCV} is needed to calculate the output power. The 2-electrode configuration is used (potential measured through the silver chloride electrodes). As for the resistance measurement, the device is filled with water and left to balance without water flux. The potential E_{OCV} is then measured until stable for several minutes.

This same configuration is used to measure the power dependency to the outer load resistor R_{load} . For each value of R_{load} , the circuit is closed and the potential drop E_R across the load resistor is measured. From the potential drop across the resistor, the power P generated by the circuit for this R_{load} value is calculated : $P = E_R^2/R_{load}$.

Acknowledgment

The authors warmly thank Prof. Yoav Green for the fruitful discussions about the theoretical modeling of our experimental results.

TD acknowledges funding from the Institut Pierre-Gilles de Gennes (laboratoire d'excellence PSL).

Author Contributions

TD, CT, AC designed the experiments. TD performed the measurements. TD, CT, AC analyzed and discussed the data. TD, CT, AC discussed the modeling. TD, CT, AC wrote, reviewed and edited the manuscript.

Conflicts of interest

There are no conflicts to declare.

Notes and references

- Bruce E. Logan and Menachem Elimelech. Membrane-based processes for sustainable power generation using water. *Nature*, 488(7411):313–319, 2012.
- Ngai Yin Yip, Doriano Brogioli, Hubertus V. M. Hamelers, and Kitty Nijmeijer. Salinity Gradients for Sustainable Energy: Primer, Progress, and Prospects. *Environmental Science & Technology*, 50(22):12072–12094, November 2016.
- Marc Pascual, Nicolas Chapuis, Soufiane Abdelghani-Idrissi, Marie-Caroline Julien, Alessandro Siria, and Lyderic Bocquet. Waste heat recovery using thermally responsive ionic liquids through nanopore and macroscopic membranes. *Energy Environ. Sci.*, pages –, 2023.
- Nan Wu, Youcef Brahmı, and Annie Colin. Fluidics for energy harvesting: From nano to milli scales. *Lab on a Chip*, 23(5):1034–1065, March 2023.
- Menachem Elimelech and William A. Phillip. The Future of Seawater Desalination: Energy, Technology, and the Environment. *Science*, 333(6043):712–717, August 2011.
- Sophie Marbach and Lydéric Bocquet. Osmosis, from molecular insights to large-scale applications. *Chemical Society Reviews*, 48(11):3102–3144, 2019.
- Mohamed Essalhi, Ahmet Halil Avci, Frank Lipnizki, and Naser Tavajohi. The potential of salinity gradient energy based on natural and anthropogenic resources in Sweden. *Renewable Energy*, 215(November 2022):118984, 2023.
- O. A. Alvarez-Silva, A. F. Osorio, and C. Winter. Practical global salinity gradient energy potential. *Renewable and Sustainable Energy Reviews*, 60:1387–1395, 2016.
- Energy institute. *Statistical Review of World Energy 2023*. 2023.
- J. Veerman, R.M. de Jong, M. Saakes, S.J. Metz, and G.J. Harmsen. Reverse electrodialysis: Comparison of six commercial membrane pairs on the thermodynamic efficiency and power density. *Journal of Membrane Science*, 343(1):7–15, 2009.
- Zhijun Jia, Baoguo Wang, Shiqiang Song, and Yongsheng Fan. Blue energy: Current technologies for sustainable power generation from water salinity gradient. *Renewable and Sustainable Energy Reviews*, 31:91–100, 2014.
- Zhizhang Yuan, Lixin Liang, Qing Dai, Tianyu Li, Qilei Song, Huamin Zhang, Guangjin Hou, and Xianfeng Li. Low-cost hydrocarbon membrane enables commercial-scale flow batteries for long-duration energy storage. *Joule*, 6(4):884–905, 2022.
- Jin Gi Hong, Bopeng Zhang, Shira Glabman, Nigmet Uzal, Xiaomin Dou, Hongguo Zhang, Xiuzhen Wei, and Yongsheng Chen. Potential ion exchange membranes and system performance in reverse electrodialysis for power generation: A review. *Journal of Membrane Science*, 486:71–88, 2015.
- Ying Mei and Chuyang Y. Tang. Recent developments and future perspectives of reverse electrodialysis technology: A review. *Desalination*, 425(September 2017):156–174, 2018.
- Gregorio Laucirica, María Eugenia Toimil-Molares, Christina Trautmann, Waldeemar Marmisollé, and Omar Azzaroni. Nanofluidic osmotic power generators – advanced nanoporous membranes and nanochannels for blue energy harvesting. *Chemical Science*, 2021.
- Hongli Yang, Viktor Gueskine, Magnus Berggren, and Isak Engquist. Cross-Linked Nanocellulose Membranes for Nanofluidic Osmotic Energy Harvesting. *ACS Applied Energy Materials*, 5(12):15740–15748, 2022.
- Xuejiao Lin, Yangjin Dong, Shenming Tao, Xiao Feng, Xijun Wang, Tao Song, Jun Liu, Zhihai Zhong, Yinchu Wang, and Haisong Qi. Temperature-gated nanocellulose membrane for enhanced and controllable osmotic energy harvesting. *Nano Energy*, 107(December 2022):108156, 2023.
- Mengyao Gao, Min Jie Zheng, Ahmed F.M. EL-Mahdy, Chen Wei Chang, Yu Chun Su, Wen Hsin Hung, Shiao Wei Kuo, and Li Hsien Yeh. A bioinspired ionic diode membrane based on sub-2 nm covalent organic framework channels for ultrahigh osmotic energy generation. *Nano Energy*, 105(August 2022):108007, 2023.
- Shangfa Pan, Peng Liu, Qi Li, Bin Zhu, Xueli Liu, Junchao Lao, Jun Gao, and Lei Jiang. Toward Scalable Nanofluidic Osmotic Power Generation from Hypersaline Water Sources with a Metal–Organic Framework Membrane. *Angewandte Chemie - International Edition*, 62(19), 2023.
- Chih-yuan Lin, Shao-fu Chang, Kuan-ting Kuo, Sean Garner, Scott C Pollard, Shih-hsun Chen, and Jyh-Ping Hsu. Essence of the Giant Reduction of Power Density in Osmotic Energy Conversion in Porous Membranes: Importance of Testing Area. *ACS Applied Materials and Interfaces*, aug 2023.
- Martin Z. Bazant, Kevin T. Chu, and B. J. Bayly. Current-voltage relations for electrochemical thin films. *SIAM Journal on Applied Mathematics*, 65(5):1463–1484, 2005.
- Yoav Green, Shahar Shloush, and Gilad Yossifon. Effect of geometry on concentration polarization in realistic heterogeneous permselective systems. *Physical Review E - Statistical, Nonlinear, and Soft Matter Physics*, 89(4):1–9, 2014.
- Yoav Green, Ran Eshel, Sinwook Park, and Gilad Yossifon. Interplay between Nanochannel and Microchannel Resistances. *Nano Letters*, 16(4):2744–2748, 2016.

- 24 John Sebastian and Yoav Green. Electrical Circuit Modeling of Nanofluidic Systems. *Advanced Physics Research*, 2300044, 2023.
- 25 James E. Hall. Access resistance of a small circular pore. *Journal of General Physiology*, 66(4):531–532, 1975.
- 26 Ahmet H. Avci, Diego A. Messina, Sergio Santoro, Ramato Ashu Tufa, Efrem Curcio, Gianluca Di Profio, and Enrica Fontananova. Energy harvesting from brines by reverse electrodialysis using nafion membranes. *Membranes*, 10(8):1–16, 2020.
- 27 A. Lindheimer, J. Molenat, and C. Gavach. A study of the supers- perfluorosulfonic membranes of Nafion perfluorosulfonic membranes. *Electroanalytical Chemistry and Interfacial Electrochemistry*, 216:71–88, 1987.
- 28 Albert Lehmani, Pierre Turq, Michelle Périé, Jacques Périé, and Jean Pierre Simonin. Ion transport in Nafion® 117 membrane. *Journal of Electroanalytical Chemistry*, 428(1-2):81–89, 1997.
- 29 Khadija Yazda, Katarina Bleau, Yuning Zhang, Xavier Capaldi, Thomas St-Denis, Peter Grutter, and Walter W. Reisner. High Osmotic Power Generation via Nanopore Arrays in Hybrid Hexagonal Boron Nitride/Silicon Nitride Membranes. *Nano Letters*, 21(10):4152–4159, 2021.
- 30 Yanjun Fu, Xun Guo, Yihan Wang, Xinwei Wang, and Jianming Xue. An atomically-thin graphene reverse electrodialysis system for efficient energy harvesting from salinity gradient. *Nano Energy*, 57(December 2018):783–790, 2019.
- 31 Hao Wang, Liangmei Su, Mehmet Yagmurcukardes, Jiawei Chen, Yu Jiang, Zhe Li, Anchang Quan, Francois M. Peeters, Cheng Wang, Andre K. Geim, and Sheng Hu. Blue Energy Conversion from Holey-Graphene-like Membranes with a High Density of Subnanometer Pores. *Nano Letters*, 20(12):8634–8639, 2020.
- 32 Jinlei Yang, Bin Tu, Guangjie Zhang, Pengchao Liu, Kui Hu, Jiarong Wang, Zhuang Yan, Zhiwei Huang, Munan Fang, Junjun Hou, Qiaojun Fang, Xiaohui Qiu, Lianshan Li, and Zhiyong Tang. Advancing osmotic power generation by covalent organic framework monolayer. *Nature Nanotechnology*, 17(6):622–628, 2022.
- 33 Xue Liu, Meng He, Dario Calvani, Haoyuan Qi, Karthick B.Sai Sankar Gupta, Huub J.M. de Groot, G. J. Agur Sevink, Francesco Buda, Ute Kaiser, and Grégory F. Schneider. Power generation by reverse electrodialysis in a single-layer nanoporous membrane made from core–rim polycyclic aromatic hydrocarbons. *Nature Nanotechnology*, 15(4):307–312, 2020.
- 34 Wesley Gould and Philip Taylor. A simulation study of ion concentration, electric potential and ion current within nafion.
- 35 Shuhua Ma, Zyun Siroma, and Hirokazu Tanaka. Anisotropic Conductivity Over In-Plane and Thickness Directions in Nafion-117. *Journal of The Electrochemical Society*, 153(12):A2274, 2006.